REVISION 2

The high pressure behavior of bloedite: a synchrotron single crystal X-ray diffraction study

PAOLA COMODI[1], SABRINA NAZZARENI[1], TONCI BALIĆ-ŽUNIĆ [2], AZZURRA ZUCCHINI [1], MICHAEL HANFLAND [3]

1 - Dipartimento di Scienze della Terra, Università di Perugia, Perugia, Italy

2 - Natural History Museum of Denmark, University of Copenhagen, Copenhagen, Denmark

3 - ESRF, Grenoble, France

Running title: *High pressure behavior of bloedite*

ABSTRACT

High-pressure single-crystal synchrotron X-ray diffraction was carried out on a single crystal of bloedite compressed in a diamond anvil cell. The volume-pressure data, collected up to 11.2 GPa, were fitted by a second and a third-order Birch-Murnaghan equations of state (EOS), yielding V_0 = 495.6(7) Å^3 with K_0 = 39.9(6) GPa, and V_0 = 496.9(7) Å^3, K_0 = 36(1) GPa and K' = 5.1 (4) GPa^{-1} respectively. The axial moduli were calculated using a Birch-Murnaghan EOS truncated at the second order, fixing K' equal to 4, for *a* and *b* axes and a third order Birch-Murnaghan EOS for *c* axis. The results were a_0 = 11.08(1) and K_0 = 56(3) GPa, b_0 = 8.20(2) and K_0 = 43(3) GPa and c_0 = 5.528(5), K_0 = 40(2) GPa, K' = 1.7(3) GPa^{-1}. The values of the compressibility for *a*, *b* and *c* axes are β_a = 0.0060(3) GPa^{-1}, β_b = 0.0078(5)GPa^{-1}, β_c = 0.0083 (4) GPa^{-1} with an anisotropic ratio of β_a:β_b:β_c = 0.72:0.94:1. The evolution of crystal lattice and geometrical parameters indicates no phase transition up to 11 GPa. Sulphate polyhedra are incompressible, whereas Mg polyhedral bulk modulus is 95 GPa. Sodium polyhedron is the softest part of the whole structure with a bulk modulus of 41 GPa. Pressure decreases significantly the distortion of Na coordination. Up to 10 GPa, the donor-acceptor oxygen distances decrease significantly and the difference between the two water molecules decreases with an increase in the strengths of hydrogen bonds. At the same time, the bond lengths from Na and Mg to oxygens of the water molecules decrease faster than other bonds to these cations suggesting that there is a coupling between the Na-Ow and Mg-Ow bond strengths and the "hydrogen transfer" to acceptor oxygens.

Keywords: bloedite, high pressure, single-crystal X-ray diffraction, equation of state

INTRODUCTION

Blodite is part of a group of sodium metal sulphate tetrahydrate minerals, with general formula $Na_2M(SO_4)_24H_2O$, where M is Mg in bloedite ($Na_2Mg(SO_4)_2{\cdot}4H_2O$), Ni in nickelbloedite, $Na_2(Ni,Mg)(SO_4)_2.4H_20$, (Nickel and Bridge 1977), and Zn in changoite, $Na_2Zn(SO_4)_24H_2O$, (Schlueter et al. 1999). Moreover, synthetic members are known with M = Co (Stoilova and Wildner 2004) and M = Fe (Hudak et al. 2008).

The bloedite crystal structure was solved by Rumanova (1958) and a structure refinement of the cobalt analogue from neutron data was done by Bukin and Nozik (1975). Later, Hawthorne (1985a) refined the structure giving a more detailed examination. The structure of bloedite is monoclinic, space group $P2_1/a$, Z=2, and is built of (001) layers of $MgO_2(H_2O)_4$ and $NaO_4(H_2O)_2$ octahedra, interconnected through SO_4 tetrahedra and hydrogen bonds (Vizcayno & Garcia-Gonzales 1999). Blodite is part of a group of sodium metal sulphate tetrahydrate minerals, with general formula $Na_2M(SO_4)_24H_2O$, where M is Mg in bloedite, Ni in nickelbloedite (Nickel and Bridge 1977), and Zn in changoite (Schlueter et al. 1999). Moreover, synthetic members are known with M = Co (Stoilova and Wildner, 2004) and Fe (Hudak et al. 2008).

Bloedite group belongs to the broader group of structures whose crystal structures are based on a finite trans $[^{VI}M(^{IV}TO_4)_2\Phi_4]$ clusters following the Hawthorne's classification of the $^{VI}M^{IV}T_2\Phi_n$ minerals (Hawthorne 1985b). The other members of the broader group are anapaite $Ca[Fe^{2+}(PO_4)_2(H_2O_4)$ (Catti et al. 1979), leonite $K_2[Mg(SO_4)_2(H_2O_4)$ (Srikanta et al. 1968) and schertelite $(NH_4)_2[Mg(PO_3OH)_2(H_2O_4)$ (Khan and Baur 1972). In all four types of structures the clusters $[^{VI}M(^{IV}TO_4)_2\Phi_4]$ play the role of fundamental building blocks (FBB) (Hawthorne 1985b) which are arranged in open sheets and bonding within and between the sheets involves both hydrogen bonds and large low-valence cations.

In bloedite FBB is $[Mg(SO_4)_2\ 4(H_2O)]^{2-}$ which is repeated by glide symmetry planes to form open sheets parallel to (001) and linked together by octahedrally coordinated Na and a complex inter-FBB hydrogen bonding (Fig. 1a and Fig 1b).

The open sheets of FBB in bloedite, anapaite, leonite and schertelite differ in the relative rotations of FBB influenced by the adjustment of low-valence cations and enabled by the flexibility of the open sheets (Hawthorne 1985b).

Bloedite is a common mineral in evaporitic sediments, in particular sodium sulphate deposits, which are usually related to non-marine environments. In sedimentology, the textural study of bloedite-rich formations is applied to extract additional information from salt beds in lacustrine sequences (Mees et al. 2011) as well as to better understand the origin of sodium sulfate deposits of economic value (e.g. Bertram, Laguna de Rey; Garrett 2001).

Bloedite is of a definite interest for planetology as one of the phases in the system H_2O-$MgSO_4$-Na_2SO_4. Clark (1980) suggested the possibility that hydrated minerals were the source of the spectral bands observed in the Galilean satellites from several space missions . McCord et al. (1999) tested possible combination of minerals that provides a good fit to the registered spectra and proposed various combinations of hydrated salts of Na and Mg: natron, mirabilite, epsomite, hexahydrite, bloedite. Nakamura and Ohtani (2011) determined the phase relations in the $MgSO_4$-H_2O binary system using an externally heated diamond anvil cell at temperatures between 298 and 500 K and pressures up to 4 GPa. Their results suggest that there may be a deep internal ocean at a depth between 200 and 1000 Km in the interior of Ganymede. However, a more complex chemical composition of the icy planets must be inferred more complex and the properties of mixed sulphate salts under high pressure are interesting in this context.

This paper represents the first high pressure study of this class of compounds, and intends to investigate the H*P* behavior of bloedite in order to determine the equation of state (EoS), the density change and evolution of crystal structure. In addition, a comparison of the evolution of

hydrogen bonds with pressure is compared to another hydrous sulphate (gypsum) whose structural change under high pressure has also been investigated in detail.

EXPERIMENTS AT ROOM PRESSURE

A natural sample of bloedite from the Natural History Museum of Denmark No. 1922.144 from Leopoldshall, Strassfurt, Germany, was selected for this investigation. The sample was chemically characterized by using a LEO 1525 – ZEISS field emission electron microscope equipped with a GEMINI column installed at the Perugia University using 15 kV accelerating voltage and 10 nA beam current. The sample appears to be chemically homogeneous and the chemical composition averaged over ten points was: SO_3.= 48.5%, Na_2O = 15.8 % and MgO = 13.7 wt%. The amount of H_2O (22 wt%) was obtained by thermogravimetric analysis. The sample was tested with an Xcalibur (Agilent Technologies) single-crystal diffractometer equipped with a CCD detector , operating at 50 KV and 40 mA and using graphite monochromated Mo radiation ($\lambda_{K\alpha 1}$ = 0.7093 Å). Diffraction data were collected at room conditions from a crystal fragment (100x80x60 μm) in air using a combination of ω and φ scans, with a step size of 0.4° and a counting time of 30 s/frame for a total of 1800 frames to maximize the reciprocal space coverage. Data were corrected for absorption with the program SADABS (Sheldrick 1996).

The crystal structure refinement was carried out with anisotropic displacement parameters using the SHELXL- program (Sheldrick 2008), starting from the atomic coordinates of Hawthorne (1985a). Neutral atomic scattering factors and $\Delta f'$, $\Delta f''$ coefficients from International Tables for Crystallography (Wilson and Prince 1999) were used. The hydrogen atoms were localized in the difference electronic density map and included in the last cycles of refinement with equal isotropic atomic displacement factors . At the end of the refinement, no peaks larger than 0.9 *e*./Å^3 were

118 present in the final difference Fourier synthesis. Details of data collection and refinement are in
119 Table 1. Table 2[1] lists the observed and calculated structure factors. Refined cell parameters, atomic
120 coordinates and displacement factors are listed in Table 3 and Table 4.
121
122 **HIGH-PRESSURE EXPERIMENTS**
123
124 The H*P* synchrotron single-crystal X-ray diffraction experiments were carried out at ID-09
125 beamline dedicated to the determination of structural properties of solids at high pressure using
126 angle-dispersive-diffraction with Diamond Anvil Cells (DAC) at ESRF (Grenoble). A membrane-
127 type DAC equipped with 300 micron diamond culets was used. Helium was used as pressure
128 transmitting medium, to carry out the measurements under hydrostatic pressure. The choice of the
129 hydrostatic medium was based on results of Singh (2012) who showed that the strength of solid
130 helium under high pressure, responsible for non-hydrostatic stresses that can develop in the sample,
131 remains very low at pressures below 20GPa, in comparison with the strength of argon, another
132 usually used medium, which acquires several times the strength of helium.
133 Ruby chip was loaded as *P* calibrant together with the bloedite sample (30x30x20 μm) in the pre-
134 indented Inconel steel gasket with a 80 μm hole. Pressure was measured before and after each data
135 collection. The X-ray beam was monochromatized to a wavelength of 0.4133 Å and focused down
136 to 5x5 μm area. Data were collected rotating the DAC of 60° round the ω-axis (from -30 to +30°)
137 with an angular step of 2° and counting time of 2s per step. The scattered radiation was collected by
138 a Mar555 flat panel detector, which has a 430 x 350 mm (555mm diagonal) active area.

1

Deposit item AM-..... Table 2 (observed and calculated structure factors). Deposit items are available two ways: For a paper copy contact the Business Office of the Mineralogical Society of America (see inside front cover of recent issue) for price information. For an electronic copy visit the MSA web site at http://www.minsocam.org, go to the American Mineralogist Contents, find the table of contents for the specific volume/issue wanted, and then click on the deposit link there.

The extraction and correction of the intensity data, merging of reflections, and the refinements of the crystal lattice parameters were done with the CrysAlis program (Agilent technologies) for the whole set of measurements (12 data collections).

The structure refinements were carried out with SHELXL (Sheldrick 2008) integrated into the WingX system, on F^2, starting from atomic coordinates of the non-hydrogen atoms from Hawthorne (1985a). Due to difficulties in performing satisfactory structure refinements, data collected at 2.07GPa, 5.95 GPa and 11.2 GPa were not finally processed. Scattering curves for neutral atoms were used. The insufficient quality of the data and the reduced number of reflections due to the diamond anvil cell, prevented us from refining the H positions.

Table 1 summarizes details of data collections and structure refinements up to 11.2 GPa. Table 2[2] lists the observed and calculated structure factors. Final atomic coordinates and isotropic displacement factors are listed in Table 5. Bond lengths, polyhedral volumes and O_{donor}-$O_{acceptor}$ distances at different pressures, are reported in Table 6.

RESULTS

RESULTS AT AMBIENT PRESSURE

The refined data at ambient conditions are in very good agreements with literature data (Hawthorne 1985a; Vizcayno & Garcia-Gonzales 1999).

The sulfur coordination tetrahedron and magnesium coordination octahedron are quite regular (Table 6), considering the volume-based distortion parameters (Balić-Žunić 2007) for the tetrahedron the arrangement of oxygen atoms is practically ideal (the volume distortion is only

2

Deposit item AM-..... Table 2 (observed and calculated structure factors). Deposit items are available two ways: For a paper copy contact the Business Office of the Mineralogical Society of America (see inside front cover of recent issue) for price information. For an electronic copy visit the MSA web site at http://www.minsocam.org, go to the American Mineralogist Contents, find the table of contents for the specific volume/issue wanted, and then click on the deposit link there.

161 0.02% and the asphericity is by definition 0). The only small distortion is due to the eccentricity of
162 the central atom (S) which is 3.5%. In the case of Mg, which lies in the center of symmetry, the
163 eccentricity is zero and the only small distortions arise from the deviation of the oxygen
164 arrangement from the ideal octahedron. It is mostly expressed in the asphericity which is 2.7% and
165 less in the volume distortion of only 0.1%. Sodium is coordinated by four oxygen atoms and two
166 H_2O groups arranged in a distorted octahedral configuration (Table 6). Among the volume-based
167 distortion parameters the eccentricity is the largest (15.2%) whereas the volume distortion is 5.4%
168 and the asphericity 7.7%.

169 The hydrogen bonding system was studied by Stoilova and Wildner (2004) by using infrared
170 spectroscopic analysis. They found a different wavenumbers of uncoupled OD stretching modes
171 related to hydrogen bond of different strengths. In particular, H_2O5 forms stronger hydrogen bonds
172 than H_2O6 due to its strongest bonding to Mg and Na (Table 6).

173 The configuration of hydrogens confirms that O5 and O6 oxygens belong to water
174 molecules and are H-donors and O1 and O4 oxygens are acceptors. In this way, a local bond-
175 valence is satisfied and two strong hydrogen bonds are formed between O5-O1 and O5-O4 with
176 distances of 2.71(1) Å and 2.74(1) Å respectively (Table 6).The longest components is along the *b*
177 axis and two weaker hydrogen bonds formed between O6-O4 and O6-O1 with distances of 2.95(1)
178 Å and 2.86(1) Å respectively (Table 6).

179

180 ## COMPRESSIBILITY

181

182 The evolution of the unit-cell of bloedite with pressure is reported in Figs. 2a and 2b and
183 Table 3. The behavior of the cell parameters shows no discontinuities in the investigated pressure
184 range, and indicates that no phase transition occurs in the bloedite structure up to 11.2 GPa. The
185 volume-pressure data were fitted by a second- and a third-order Birch-Murnaghan equations-of-
186 state, using the EOSFIT-5.2 software (Angel 2002). The second-order Birch-Murnaghan EoS fit

yields V_0 = 495.6(7) Å^3 with K_0 = 39.9(6) GPa, whereas the third order Birch-Murnaghan EoS fit yields V_0 = 496.9(7) Å^3, K_0 = 36(1) GPa and K' = 5.1(4) GPa^{-1}, as from a mathematical formalism which implies a negative correlation between K and K'. The bulk modulus and the first derivative values are in agreement with the values obtained from the evolution of the "Eulerian finite strain" versus "normalized stress", namely the F_E-f_e plot (Angel 2000) showed in Figure 3. The intercept value and the slope obtained by a linear regression give $F_E(0)$ and K' values equal to 31(1) GPa and 6.8(8) GPa^{-1}, respectively.

The axial moduli for *a*, *b*, *c* lattice parameters were calculated using a Birch-Murnaghan EoS truncated at the second order, fixing K' equal to 4, for *a* and *b* axes and a third-order Birch-Murnaghan equation of state for *c* axis, in which fit is made for the cubes of the individual axes, following Angel (2002). The results were a_0 = 11.08(1) Å, K_{0a} = 56(3) GPa, b_0 = 8.20(2) Å, K_{0b} = 43(3) GPa and c_0 = 5.528(5) Å, K_{0c} = 40(2) GPa, K'_c = 1.7(3) GPa^{-1}. The respective values of the compressibilities for *a*, *b* and *c* axes obtained as the reciprocal value of three times K_0 are β_a = 0.0060(3) GPa^{-1}, β_b = 0.0078(5) GPa^{-1} and β_c = 0.0083(4) GPa^{-1} with an anisotropic ratio of β_a:β_b:β_c = 0.72: 0.94:1.

The *Win_Strain* software (Angel 2011) was used to calculate the magnitude and the orientation of the principal unit-strain coefficients in the investigated pressure range. The principal strain axes were ε_1 = 0.0052 GPa^{-1}, ε_2 = 0.0069 GPa^{-1}, ε_3 = 0.0075 GPa^{-1} with the following orientation: $\varepsilon_1 \angle$ c = 84.1°, $\varepsilon_1 \angle$ b = 90°, $\varepsilon_1 \angle$ a = 16.6°; $\varepsilon_2 \parallel$ b; $\varepsilon_3 \angle$ c = 5.9°, $\varepsilon_3 \angle$ b = 90°, $\varepsilon_3 \angle$ a = 106.6° (Fig. 1b). On the basis of the unit-strain coefficients between 1 and 11.2 GPa, the elastic behavior of bloedite is anisotropic with ε_1 :ε_2 :ε_3 = 1:1.33:1.44.

STRUCTURAL EVOLUTION WITH PRESSURE

212

213 Figure 4 shows the behavior of the average polyhedral bond distances normalized to the
214 room pressure values at different *P*. Structural refinements on nine data collections from room
215 pressure up to 10 GPa, indicate that the SO_4 tetrahedral volume and the average <S-O> bond
216 distances remain almost unchanged, with <S-O> of 1.47(1) Å (10^{-3} GPa) -1.46(1) Å (10 GPa) and
217 polyhedral volume of 1.635 $Å^3$ (10^{-3} GPa) 1.60 $Å^3$ (10 GPa). Only the S-O4 distance, along the *c*
218 axis, decreases from 1.480(1) Å to 1.46(1) at 10 GPa. These values are very close to those measured
219 for the sulphate polyhedra in gypsum by Comodi et al. (2008).

220 In the magnesium polyhedra the longest distances between Mg and O6 and O5 shorten more
221 than the shorter Mg-O3 distances (Figure 5). The average bond distance decreases from 2.07(2) Å
222 (10^{-3} GPa) to 2.00(4) Å (10 GPa) and the polyhedral volume from 11.9 $Å^3$ (10^{-3} GPa) to 10.6 $Å^3$(10
223 GPa). The distortion of the polyhedron increases weakly (the asphericity of coordination increases
224 from 2.7% to 5.4%: Table 6). The polyhedral bulk modulus is 95 GPa and it is intermediate among
225 the polyhedral bulk moduli of magnesium observed in other structures: for example in olivine,
226 pyroxenes and phlogopites, where the bulk moduli of Mg polyhedra were 100 GPa (Hazen 1976),
227 120 GPa (Levien and Prewitt 1981) and 86 GPa (Comodi et al. 2004), respectively. These data
228 indicate that the polyedral bulk modulus is not affected by the presence of oxygens or OH/water at
229 corners but may be affected by the structural arrangement. In Mg-chloritoid, Comodi et al. (1992)
230 measured a very low bulk modulus (53 GPa) for the Mg polyhedra and they associated that
231 anomalous behavior to the presence of magnesium in a large site usually occupied by iron. .

232 With a bulk modulus of 41 GPa the sodium polyhedron is softer than the other polyhedra in
233 the structure. The average <Na-O> bond distance reduces from 2.45(1) Å (10^{-3} GPa) to 2.26(6) Å
234 (10 GPa) and the difference in bond lengths decreases since the longest distance Na-O6 changes
235 faster (from 2.653(2) Å to 2.33(2) Å) than the others bond lengths (Figure 6). The distortion of the
236 coordination decreases significantly with pressure (Table 6).

Due to the difficulty in determining the positions of hydrogens under H*P* conditions by using X-ray diffraction, the hydrogen bond evolution was followed through the measurements of O_{donor}-$O_{acceptor}$ distances (Figure 7). The longest distances O6-O1 and O6-O4 [2.86(1) Å and 2.95(1) Å at 0.001 GPa], have a compressibility of 7.7(6) and 9.2(7) 10^{-4} GPa^{-1}, whereas the shortest ones, O5-O1 and O5-O4 [2.71(1) Å and 2.74(1) Å at 0.001 GPa] have a compressibility of 2.8(9) and 4.4(7)10^{-4} GPa^{-1}, respectively.

The crystal structure houses ten types of voids: a large 9-coordinated void (V1) in the form of an elongated tri-capped trigonal antiprism and a 7-coordinated void (V2) in the form of a mono-capped trigonal prism, both situated between the octahedral layers. One 6-coordinated void in the form of a trigonal prism (V3) inside the octahedral layer plus two octahedral voids, one inside the octahedral layer between the two Na polyhedra (V4) and one between the octahedral layers between the two Mg polyhedra (V5). Two 5-coordinated voids in the form of square pyramids (V6,V7), both inside the octahedral layer. Finally, three tetrahedral voids, one inside the octahedral layer (V8), and two between the layers (V9,V10). It can be seen that the main characteristic of the structure is the virtual incompressibility of the S tetrahedron (only 2% up to 10 GPa) plus that the Na octahedron is the most compressible part of the structure, save the V10 void. The latter one includes the O1, O3, O5 and O6 atoms, which means that two of its edges are formed by the two hydrogen bonds from O5 and O6 pointing to the same O1 atom. As illustrated in Figure 7, these two donor-acceptor distances, which at room pressure are significantly different, converge to a common value with pressure. The strong contraction of the corresponding face causes the decrease of the small volume of this void by almost ¼ volume up to 10 GPa.

The kinetic diameter of helium is 2.6 Å (Breck 1974) which rises the question of the possibility that helium penetrates in the structure and affects its pressurized behavior. The largest, nine-coordinated void in the structure has at room pressure the average distance of the centre to the nuclei of surrounding oxygen atoms of 2.6 Å. Taking in account that the diameter of the oxygen anion in the structure also is around 2.6 Å, this leaves a place to accommodate helium in this void,

263 but we must also note that these voids are isolated in the structure and that a penetration of helium
264 through faces made by three oxygen atoms is unrealistic. We therefore assume that the nature of
265 voids in the structure does not imply a possibility of the influence of helium penetration on
266 compressibility.
267
268
269

270 **DISCUSSION**

271 The relative compression of the various coordination polyhedra plus the voids (Fig. 8)
272 present in the arrangement of oxygen atoms can help understanding the behavior of the bloedite
273 structure under pressure. If we assume the Hawthorne's (1985a) view of the crystal structure as built
274 of FBB $[Mg(H_2O)_4(SO_4)_{2,}]^{-2}$ clusters which are interlinked by Na-polyhedra and hydrogen bonds,
275 then we can see that they behave as nearly rigid units with a small compression of the Mg
276 coordination and practically no compression of the sulphate groups. The largest part of the volume
277 decrease is taken by the Na coordinations, which compress even more than any void in the crystal
278 structure. The hydrogen bonds show different compressibility: the weaker bonds with O6 as the
279 donor atom compress 3-times more than the stronger with O5 donor atom. Since 06-01 and 06-04
280 hydrogen bonds link neighboring (001) sheets, the lattice parameter *c* is the most compressible
281 among lattice parameters.

282 The high pressure structural evolution of bloedite may be compared with that of
283 gypsum, another hydrated sulphate mineral (Comodi et al. 2008; Comodi et al. 2012). Although the
284 two structures have a quite similar bulk moduli (gypsum bulk modulus = 44(3) GPa, K'=3.3(3);
285 Comodi et al. 2008) and both show the incompressibility of sulphate tetrahedra with a high
286 compressibility of the hydrogen bonds, evolution of the structure is quite different. No phase

transition was observed up to 11.2 GPa in bloedite at room temperature, whereas gypsum undergoes a phase transition at 4 GPa (Comodi et al. 2008; Nazzareni et al. 2010).

Gypsum is a layered mineral with alternate layers of Ca- and S-polyhedral chains separated by interlayers occupied by water molecules which causes a perfect cleavage parallel to (010). However, the axial compressibility of gypsum is almost isotropic (β_{0a}:β_{0b}:β_{0c} = 1:1:0.9). To explain this behavior, Comodi et al. (2008) noted that the two consecutive structural layers parallel to (010) have very different compressibilities: the polyhedral layer is almost incompressible, whereas water layer compressibility is 9.7(3) 10^{-3} GPa^{-1}, about twice that of the *a* and *c* lattice parameters.

In bloedite the open sheets of FBBs are quite flexible and the compressibility is followed by the packing of FBBs, which gives the largest compressibility along the softest Na-O and hydrogen bonds.

In gypsum approaching the phase transition, the hydrogen bonds reach the value of 2.7 Å, which is below the non-bonded O…O contact distance, following Brown (1976). At this distance, the repulsion between oxygen atoms becomes so strong that a change in the compression mechanism might occur, as it is observed, for instance, in chlorite (Zanazzi et al. 2006; Zanazzi et al. 2007). In bloedite, up to 10 GPa, some Odonor-Oacceptor distances approach the 2.6 Å value which obviously represents a tolerable value for this structure type.

An important detail is that the most compressible hydrogen bonds (Figure 7) involve the donor atoms (O6) which, at the same time, is involved in the fastest bonds shortening to the Na and Mg atoms (Figures 6 and 5). This suggests that the "hydrogen transfer" to the acceptor O atoms and the stronger bonding of the donor atom to cations are coupled in the bloedite structure, primarily due to the changes in the Na bonding characteristics, but also in that of Mg. Note that, while the bond lengths Mg-O5 and Mg-O6 decrease significantly with pressure, the Mg-O3 bond length remains unchanged and becomes the longest one (Figure 6).

IMPLICATIONS

A result of this study is the measured increase of density of bloedite with pressure up to 11.2 GPa by about 20% (from 1.20 g/cm^3 to 1.46 g/cm^3), the FBB has a rigid behavior whereas the inter-FBB hydrogen bonding and the Na coordination polyhedra are soft. The structure is very flexible and adjusts the structural change induced by pressure increase without a phase transition. To the best of our knowledge this is the first study on the high pressure behavior of a member of the bloedite group and on minerals based on finite heteropolyhedral clusters of the form of $[^{VI}M(^{IV}TO_4)_2\Phi_4]$. We presume that the isostructural members where Mg is substituted by Fe, Ni, Co or Zn which differs in ionic radii by less than 10%, will have a very similar behavior.

A similar behavior with rigid FBB of the form $[^{VI}M(^{IV}TO_4)_2\Phi_4]$ and soft inter-FBB bonding could be expected in the other members of the broader structural group, but the flexibility of the individual structures is hard to predict and should be investigated.

The evolution of bloedite structure with pressure suggests that water remains in the crystal structure of the mineral at high-pressure conditions and room temperature up to 10 GPa and even that the hydrogen bonding of the weaker water molecule O6H2 is increased and approaches in strength that of the stronger bonded one, O5H2. It could also be expected that the pressure would increase the dehydration temperature of bloedite and in this way influence its stability in natural environments. In this respect, an IR or Raman spectroscopic study of bloedite under high pressure conditions would be of interest.

.

337
338
339
340

ACKNOWLEDGMENT

341 The European Synchrotron Facility is acknowledged for allocating beamtime for the experiment.
342 The study was supported by MIUR Italian Ministero dell'Istruzione dell'Università e della Ricerca
343 (PRIN-2010-2011 to PC). The editor Lars Ehm and two anonymous referees are acknowledged for
344 very useful and constructive comments

REFERENCES

Angel, R.J. (2000) Equation of state. In R.M. Hazen and R.T. Downs Eds. High temperature and High pressure Crystal Chemistry, 41, p. 117-211. Reviews in Mineralogy and Geochemistry, Mineralogy Society of America, Chantilly, Virginia.

Angel, R.J. (2002) EOSFIT. Crystallography Laboratory, Virginia tech, Blacksburg.

Angel, R.J. (2011) Win_Strain. Crystallography Laboratory, Virginia tech, Blacksburg.

Brown, I .D. (1976) On the geometry of O-H . . . O hydrogen bonds. .Acta Crystallographica A32, 24-3l .

Bukin, V.I. and Nozik, Yu. Z. (1975) Neutron diffraction study of the crystal structure of cobalt astrakhanite $Na_2Co(SO_4)_2.4H_2O$. Soviet Physics Crystallography, 20, 180-182.

Balić-Žunić, T. (2007) Use of three-dimensional parameters in the analysis of crystal structures under compression. In: Pressure-Induced Phase Transitions 2007, ed. Grzechnik A., pp. 157-184, Transworld Research Network, Trivandrum. ISBN: 81-7895-272-6

Breck, D.W. (1974) Zeolite Molecular Sieves: Structure, Chemistry and Use. New York . Wiley, p-636.

Catti, M., Ferraris, G., and Ivaldi, G. (1979) Refinement of the crystal structuyre of anapaite Ca2Fe(PO4)24H2O: Hydrogen bonding and relationship with bihydrated phase. Bulletin de la Societe Francaise de Mineralogie et de Cristallographie, 102, 314-318.

Clark, R. N. (1980) Ganymede, Europa, Callisto, and Saturn's rings: Compositional analysis from reflectance spectroscopy. Icarus, 44, p. 388-409.

Comodi, P., Mellini, M., and Zanazzi, P.F. (1992) Magnesiochloritoid: compressibility and high pressure structure refinement. Physics and Chemistry of Minerals, 18, 483–490.

Comodi, P., Fumagalli, P., Montagnoli, M., and Zanazzi, P.F. (2004) A single-crystal study on the pressure behavior of phlogopite and petrological implications. American Mineralogist, 89, 647-653

Comodi, P., Nazzareni, S., Zanazzi, P.F., and Speziale, S. (2008) High pressure behavior of gypsum: A single-crystal X-ray study. American Mineralogist, 93 (10), 1530-1537

Comodi, P., Kurnosov, A., Nazzareni, S., and Dubrovinsky, L. (2012) The dehydration process of gypsum under high pressure. Physics and Chemistry of Minerals, 39(1), 65-71

Garrett, D.E. (2001) Sodium Sulfate. Handbook of Deposits, Processing, Properties, and Use, Academic Press, San Diego, p. 365.

Hawthorne, F. C. (1985a) Refinement of the crystal structure of bloedite: structural similarities in the [^{VI}M(^{IV}TΦ_4) Φ_n]. Canadian Mineralogist, 23, 669-674

Hawthorne, F.C. (1985b) Towards a structural classification of minerals: The $^{VI}M^{IV}T_2\Phi_n$ minerals . Am Mineral. 70, 455-473

Hazen, R. M. (1976) Effects of temperature and pressure on the crystal structure of forsterite. American Mineralogist, 61, 1280-1293.

Hudak, M., Diaz, J.G., Kozisek, J. (2008) Disodium tetraaquabis(sulfato)iron(II). Acta Crystallographica, E64, i10

Khan, A.A., and Baur, W.H. (1972) Salt hydrates. VIII. The crystal structure of sodium ammonium orthochromates di-hydrate and magnesium di-ammonium bis (hydrogen orthophosphate) tetrahydrate and a discussion of the ammonium ion. Acta Crystallographica B28, 683-693.

Levien, L., and Prewitt, C.T. (1981) High pressure structural study of diopside. American Mineralogist, 66:315-323

McCord, T.B., Hansen, G.B., Matson, D.L., Johnson, T.V., Crowley, J.K., Fanale, F.P., Carlson, R.W., Smythe, W.D., Martin, P.D., Hibbitts, C. A., Granahan, J.C., Ocampo, A. and the NIMS Team (1999) Hydrated salt minerals on Europa's surface from the Galileo NIMS investigation. Journal of Geophysics Research, 1046, 3311-3319

393 Mees, F., Castañeda, C., Herrero, J., and Van Ranst, E. (2011) Bloedite sedimentation in a
394 seasonally dry saline lake (Salada Mediana, Spain). Sedimentary Geology, 238(1-2), 106-115
395 Nakamura, R., and Ohtani, E. (2011) The high-pressure phase relation of the MgSO4–H2O system
396 and its implication for the internal structure of Ganymede. Icarus, 211, 648-654
397 Nazzareni, S., Comodi, P., Bindi, L., and Dubrovinsky L. (2010) The crystal structure of gypsum-II
398 determined by single-crystal synchrotron X-ray diffraction data. American Mineralogist, 95 (4),
399 655-658
400 Nickel, E.H., and Bridge P.J. (1977) Nickelblödite, $Na_2Ni(SO_4)_2 \cdot 4H_2O$, a New Mineral from
401 Western Australia. Mineralogical Magazine*, 41, 37-41*
402 Rumanova, I.M. (1958) Crystal structure of bloedite. Dokladi Akademii Nauk SSSR 118, 84-87
403 Sheldrick, G.M (1996) SADABS Program for empirical absorption correction of area detector data.
404 Institut für Anorganische Chemie, University of Göttingen, Germany.
405 Sheldrick, G.M. (2008) A short history of SHELX. Acta Crystallographica, A64, 112–122
406 Singh, A.K. (2012) Strength of solid helium under high pressure. Journal of Physics: Conference
407 Series 377, 012007
408 Schlueter, J., Klaska, K.-H. and Gebhard, G. (1999) Changoite, $Na_2Zn(SO_4)_2 \cdot 4H_2O$, the zinc
409 analogue of bloedite, a new mineral from Sierra Gorda, Antofagasta, Chile. Neues Jahrbuch für
410 Mineralogie, Montashefte, 3, 97-103
411 Srikanta, S., Sequiera, A., and Chidambaram, R. (1968) Neutron diffraction study of the space
412 group and structure of manganese-leonite $K_2Mn(SO_4)_2 4H_2O$. Acta Crystallographica B24, 1176-
413 1182.
414 Stoilova, D., and Wildner, M. (2004) Bloedite-type compounds $Na_2Me(SO_4)_2\ 4H_2O$(Me = Mg, Co,
415 Ni, Zn): crystal structures and hydrogen bonding systems. Journal of Molecular Structure, 706, 57-
416 63

Wilson, A.J.C., and Prince, E. (1999) International Tables of Crystallography. Kluver Academic Publisher, 3300 AH Dordrecht, The Netherlands.

Vizcayno, C., and Garcia-Gonzales, M.T. (1999) $Na_2Mg(SO_4)2\cdot 4H_2O$, the Mg end-member of the bloedite-type of mineral. Acta Crystallographica C55, 8-11.

Zanazzi, P.F., Montagnoli, M., Nazzareni, S., and Comodi, P. (2006) Structural effects of pressure on triclinic chlorite: A single-crystal study. American Mineralogist, 91, 1871-1878

Zanazzi, P.F., Montagnoli, M., Nazzareni, S., and Comodi, P. (2007) Structural effects of pressure on monoclinic chlorite: A single-crystal study. American Mineralogist, 92, 655-661

Figure and Table Captions

Figure 1. The crystal structure of bloedite based on the structural refinement at room conditions: a) (001) projection ; b) (010) projection. Inset: (010) projection of the strain ellipsoid (see text for discussion)

Figure 2. a) The evolution of the unit cell volume data fitted by a third-order Birch-Murnaghan EoS and b) The evolution of the unit cell parameters a, b, c, β normalized to the values at room conditions as a function of pressure (GPa).

Figure 3 Evolution of the "normalized stress" F_E versus Eulerian finite strain f_E; the solid line is the weighted linear fit of the data.

441 Figure 4 Variation of the average bond distances of the S, Mg and Na at different pressures (GPa)
442 normalized to the room condition values.
443 Figure 5 Evolution with pressure (GPa) of the bond distances in the magnesium coordination
444 polyhedron (Å) .
445 Figure 6 Evolution with pressure (GPa) of the bond distances in the sodium coordination
446 polyhedron (Å).
447 Figure 7 Evolution with pressure (GPa) of the $O_{donor}...O_{acceptor}$ distances(Å)
448 Figure 8. Relative compression of various coordination polyhedra (S, Mg, Na) plus the structural
449 voids (V).
450

451 Table 1. Details of data collections and structure refinements of bloedite at different pressures.
452 Notice that data collected at 2.07 GPa, 5.95 GPa and 11.2 GPa were not included in the refinements
453 (see the text for details).

454 Table 3. Unit cell parameters, density and absorption coefficient of bloedite at different pressures.

455 Table 4. Fractional atomic coordinates and displacement parameters of bloedite obtained from data
456 collected at room pressure.

457 Table 5. Fractional atomic coordinates and displacement parameters of bloedite obtained from data
458 collected at different pressures.

459 Table 6 O_{donor}-$O_{acceptor}$ distances, polyhedral bond lengths, polyhedral volumes and distortion
460 parameters in bloedite at different pressures. asp = asphericity, vd = volume distortion, ecc =
461 eccentricity, all values normalized to the same volume scale (Balic-Zunic 2007). For Mg (lying in
462 the centre of symmetry) the eccentricity is by definition 0 and for the S (tetrahedral coordination)
463 the asphericity is by definition 0.
464

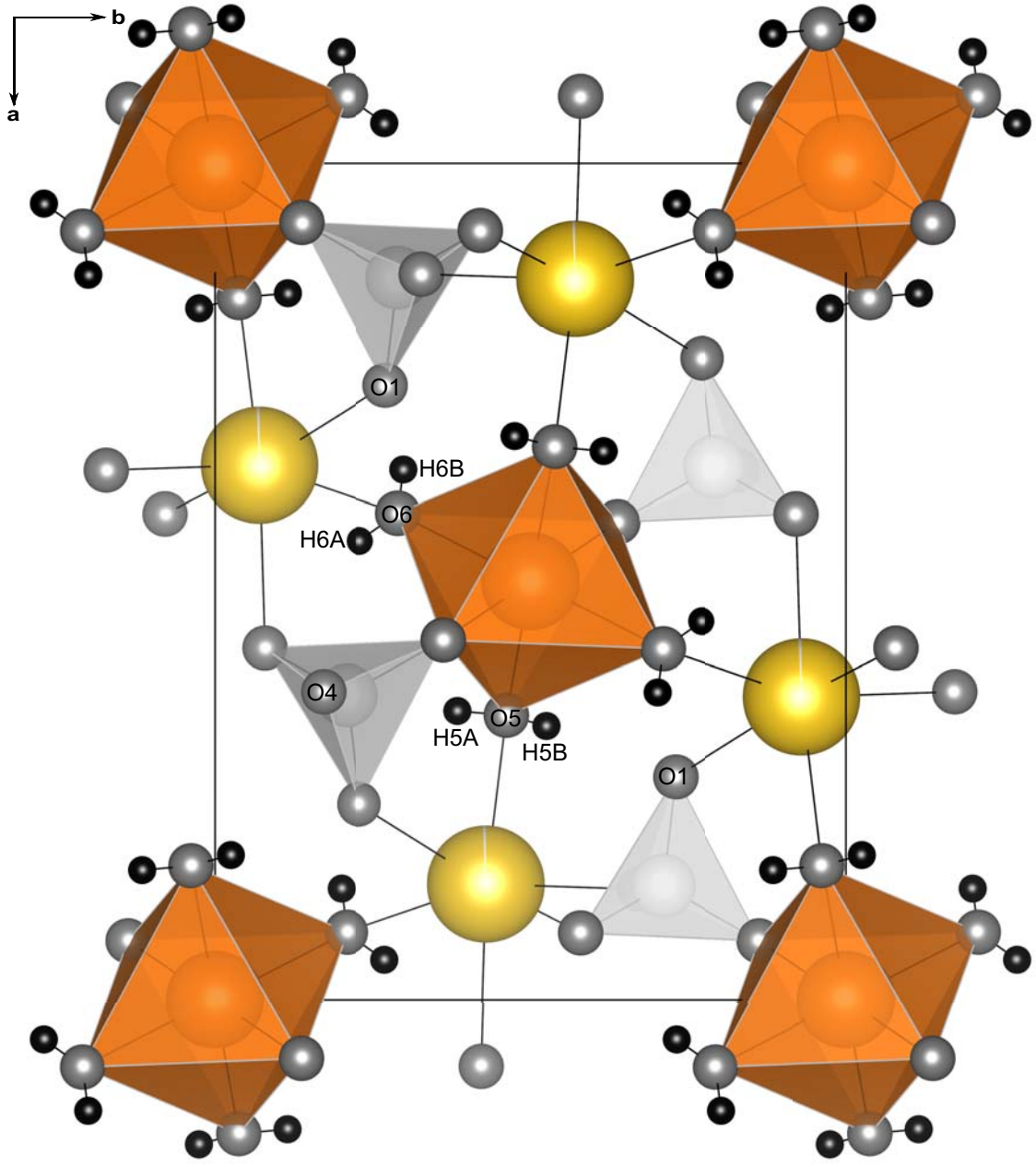
b
a
O1
H6B
O6
H6A
O4
O5
H5A
H5B
O1

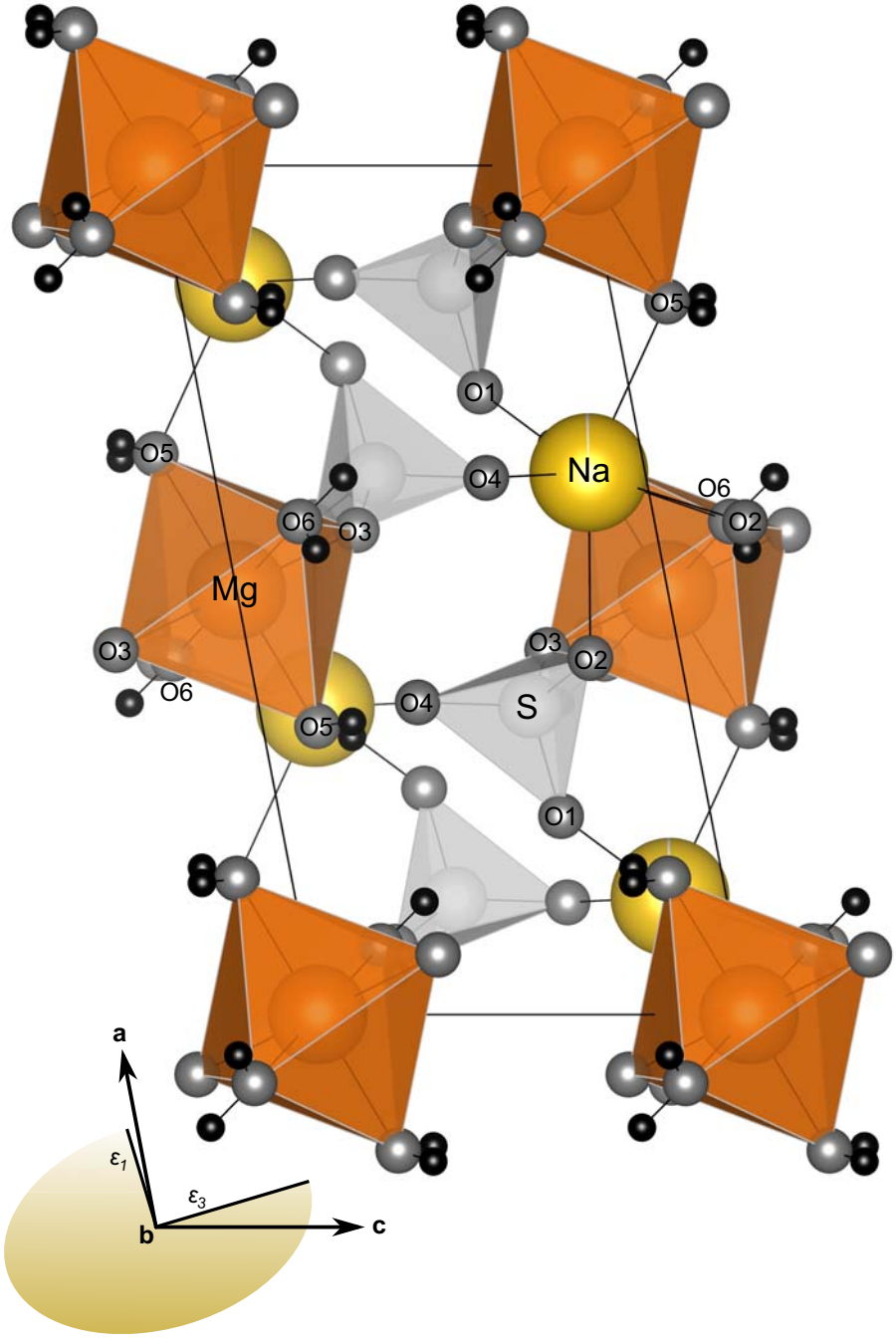
O5
O1
O5
Na
O4
O6
O6
O2
O3
Mg
O3
O3
O2
O6
O4
S
O5
O1
a
ε1
ε3
b
c

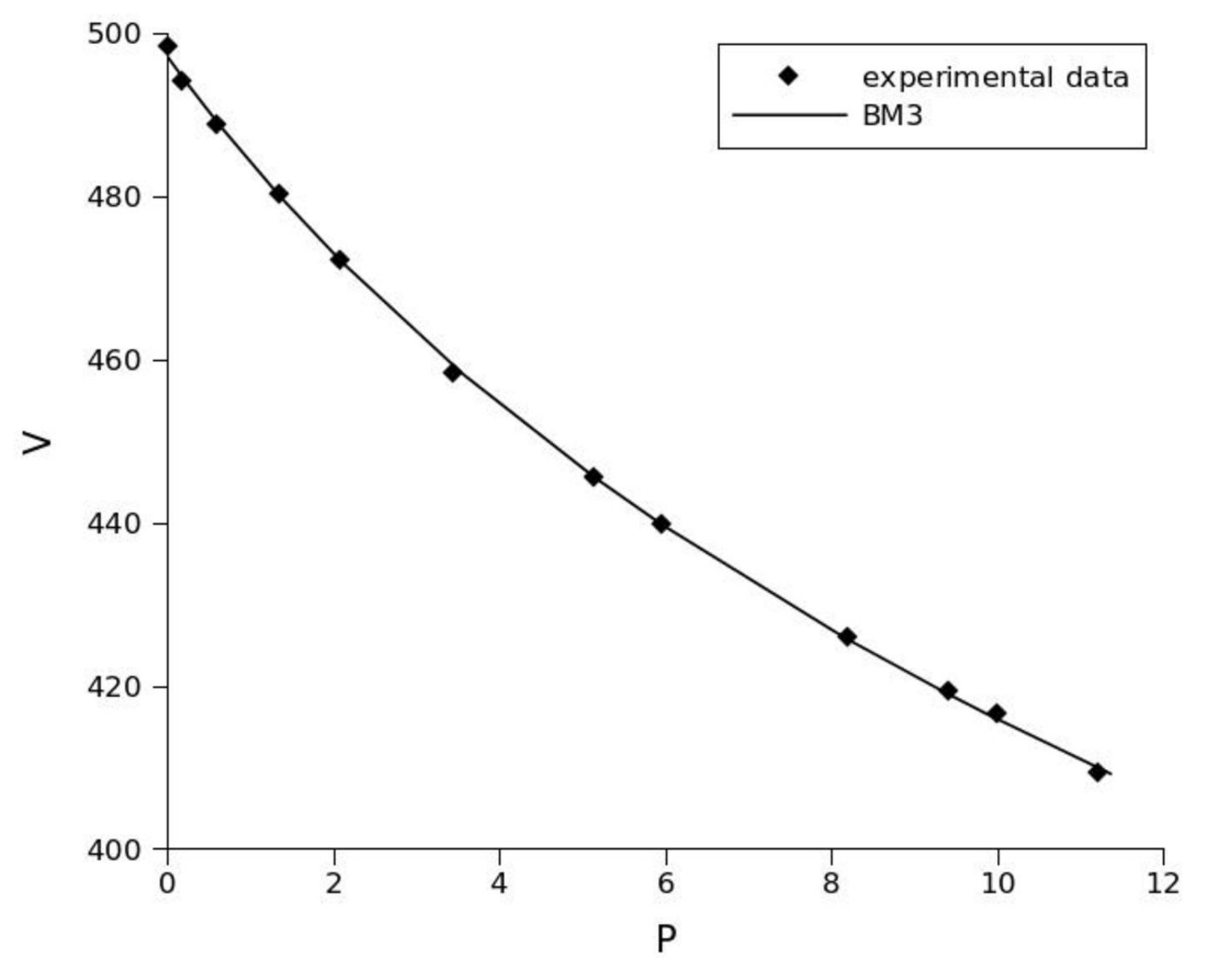
experimental data
BM3
V
P
500
480
460
440
420
400
0
2
4
6
8
10
12

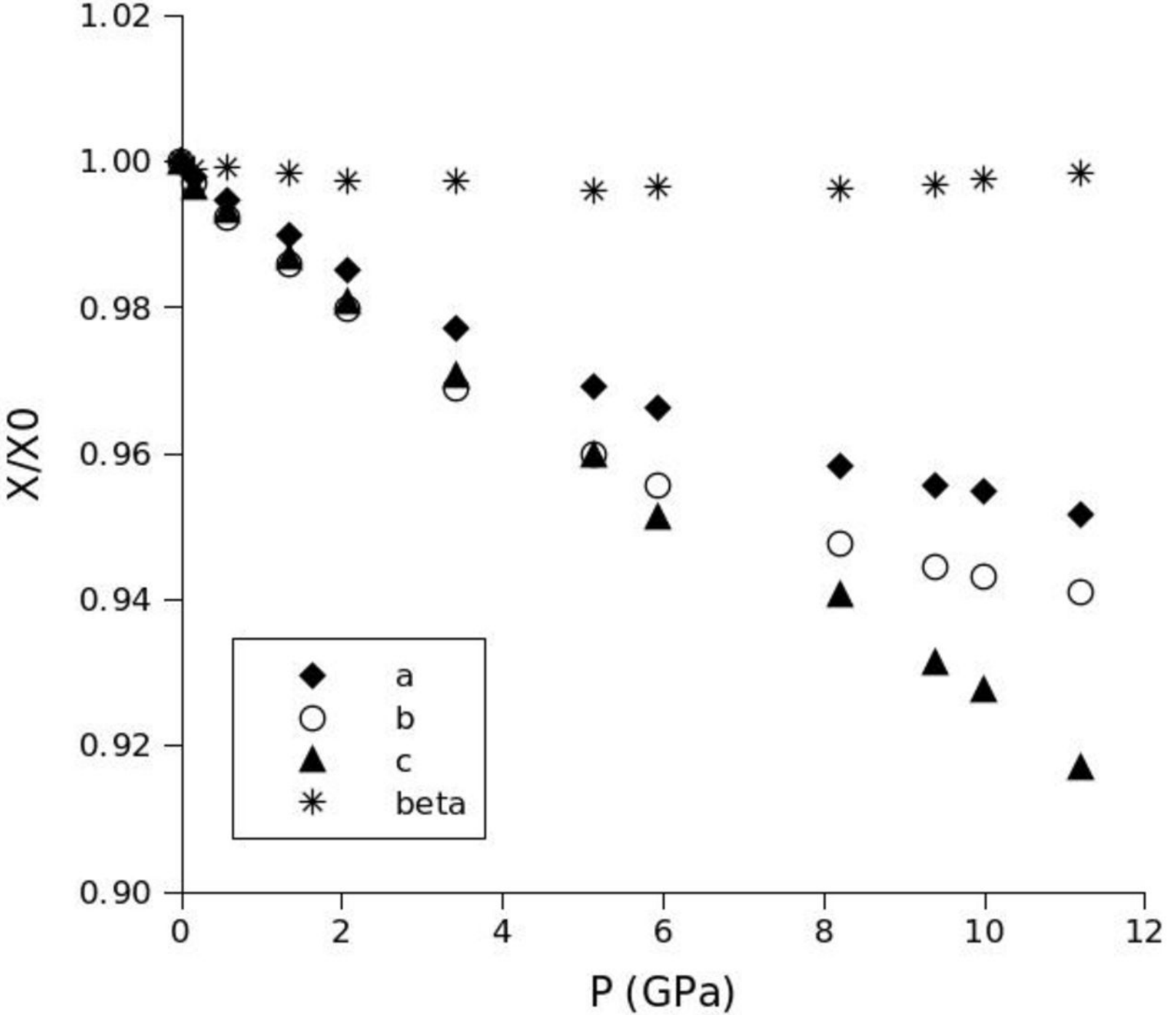
1.02
1.00
0.98
0.96
0.94
0.92
0.90
X/X0
0
2
4
6
8
10
12
P (GPa)
a
b
c
beta

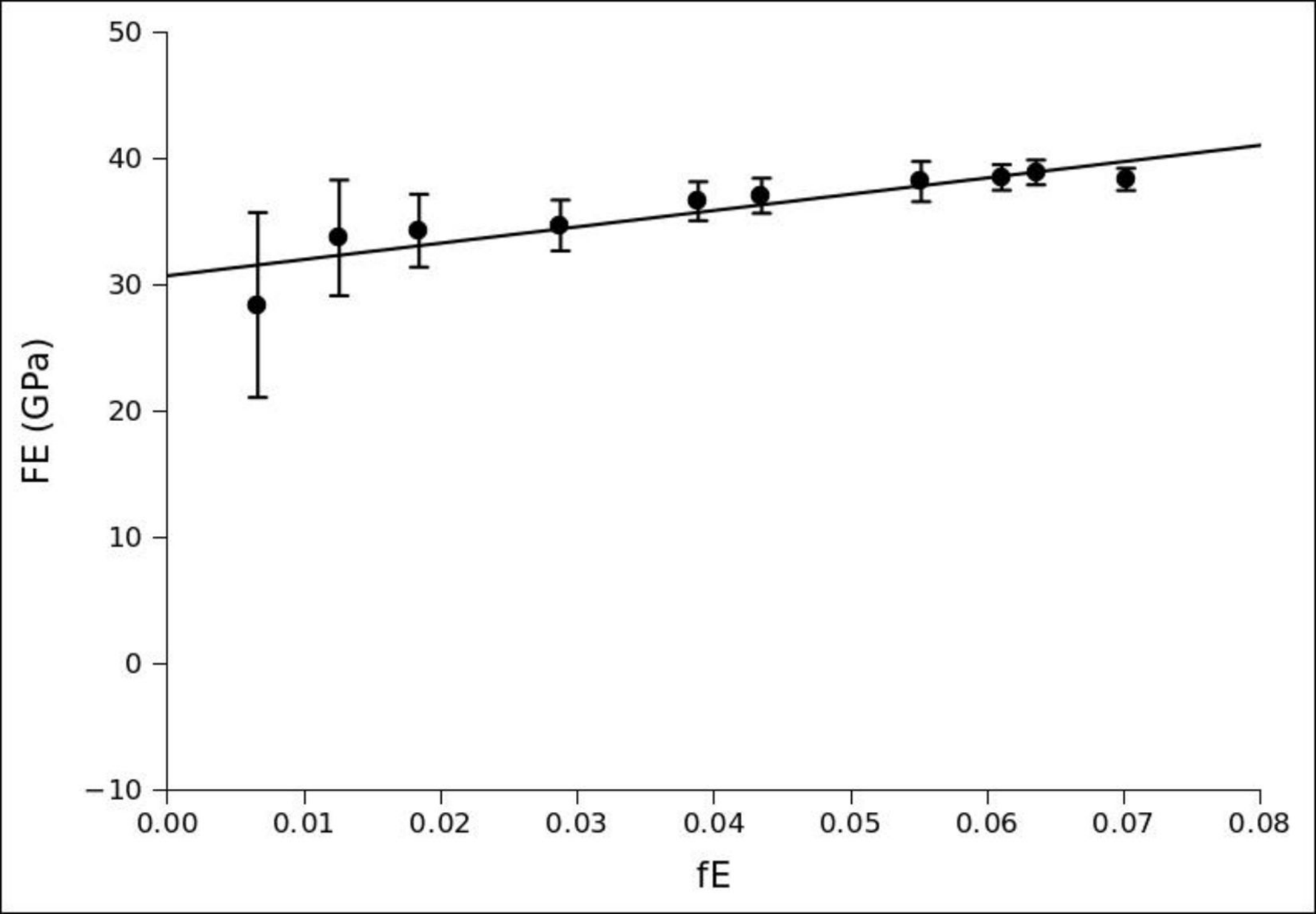
50
40
30
20
10
0
−10
FE (GPa)
0.00
0.01
0.02
0.03
0.04
0.05
0.06
0.07
0.08
fE

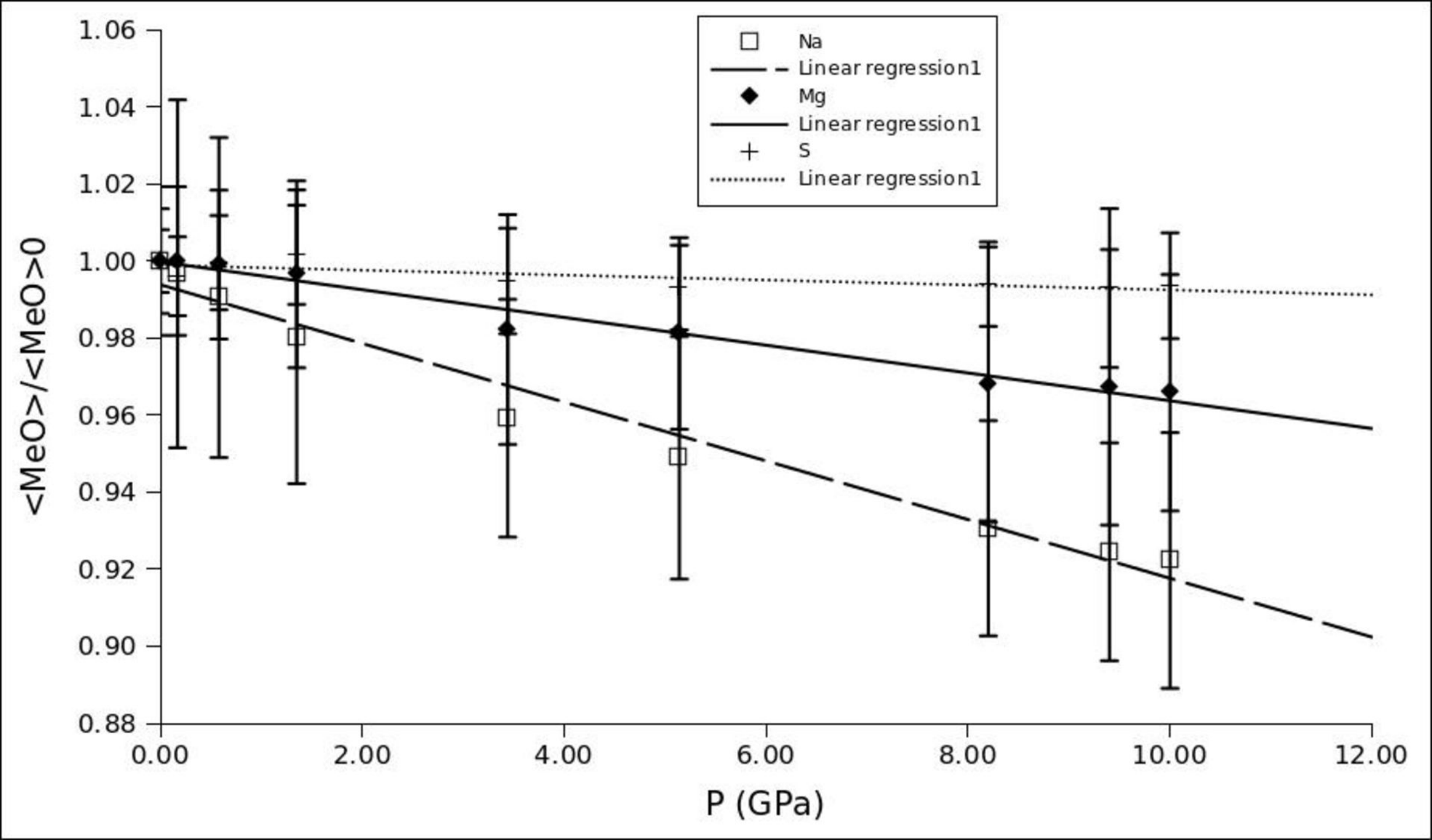
Na
Linear regression1
Mg
Linear regression1
S
Linear regression1
1.06
1.04
1.02
1.00
0.98
0.96
0.94
0.92
0.90
0.88
<MeO>/<MeO>0
0.00
2.00
4.00
6.00
8.00
10.00
12.00
P (GPa)

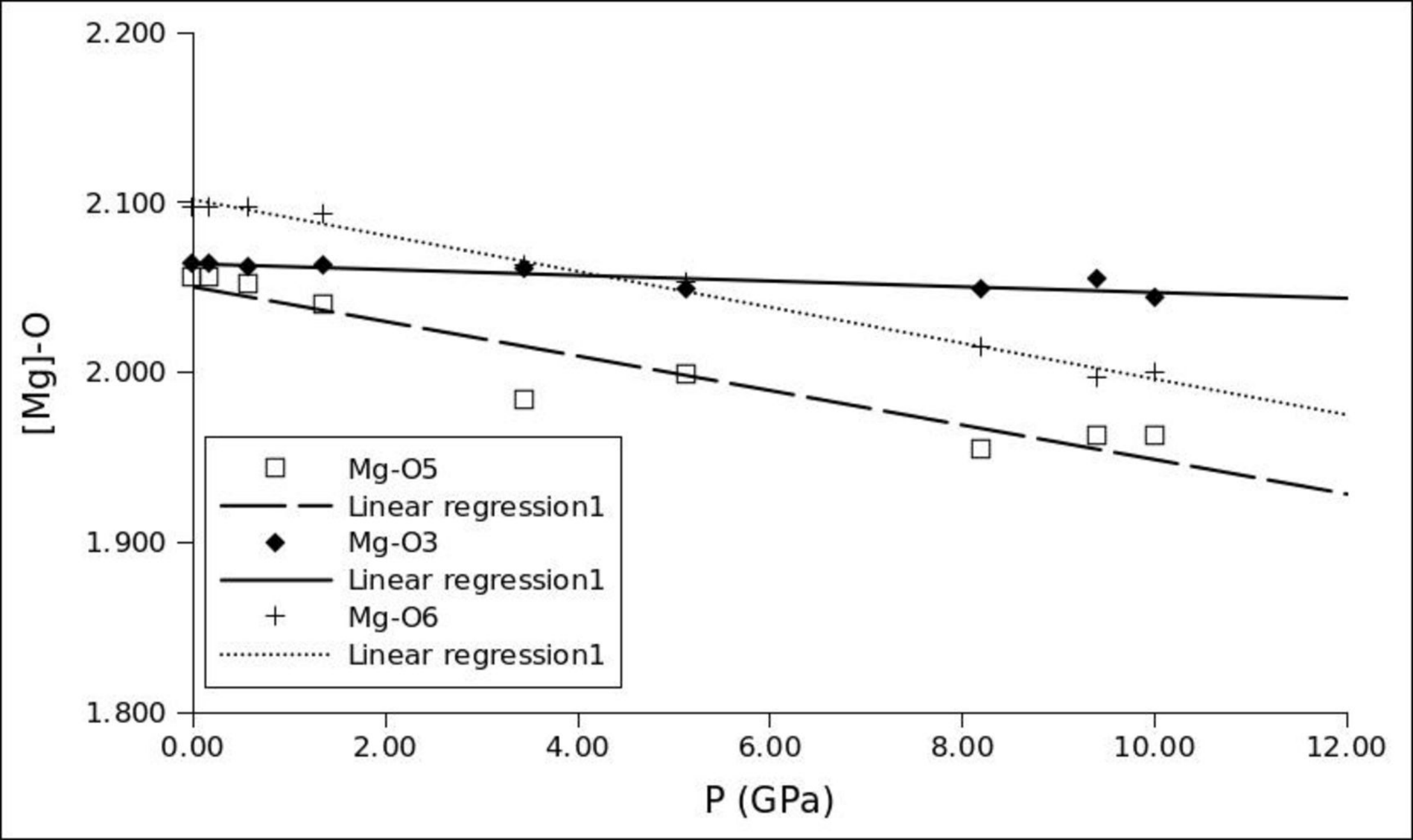
2.200
2.100
2.000
1.900
1.800
[Mg]-O
0.00
2.00
4.00
6.00
8.00
10.00
12.00
P (GPa)
Mg-O5
Linear regression1
Mg-O3
Linear regression1
Mg-O6
Linear regression1

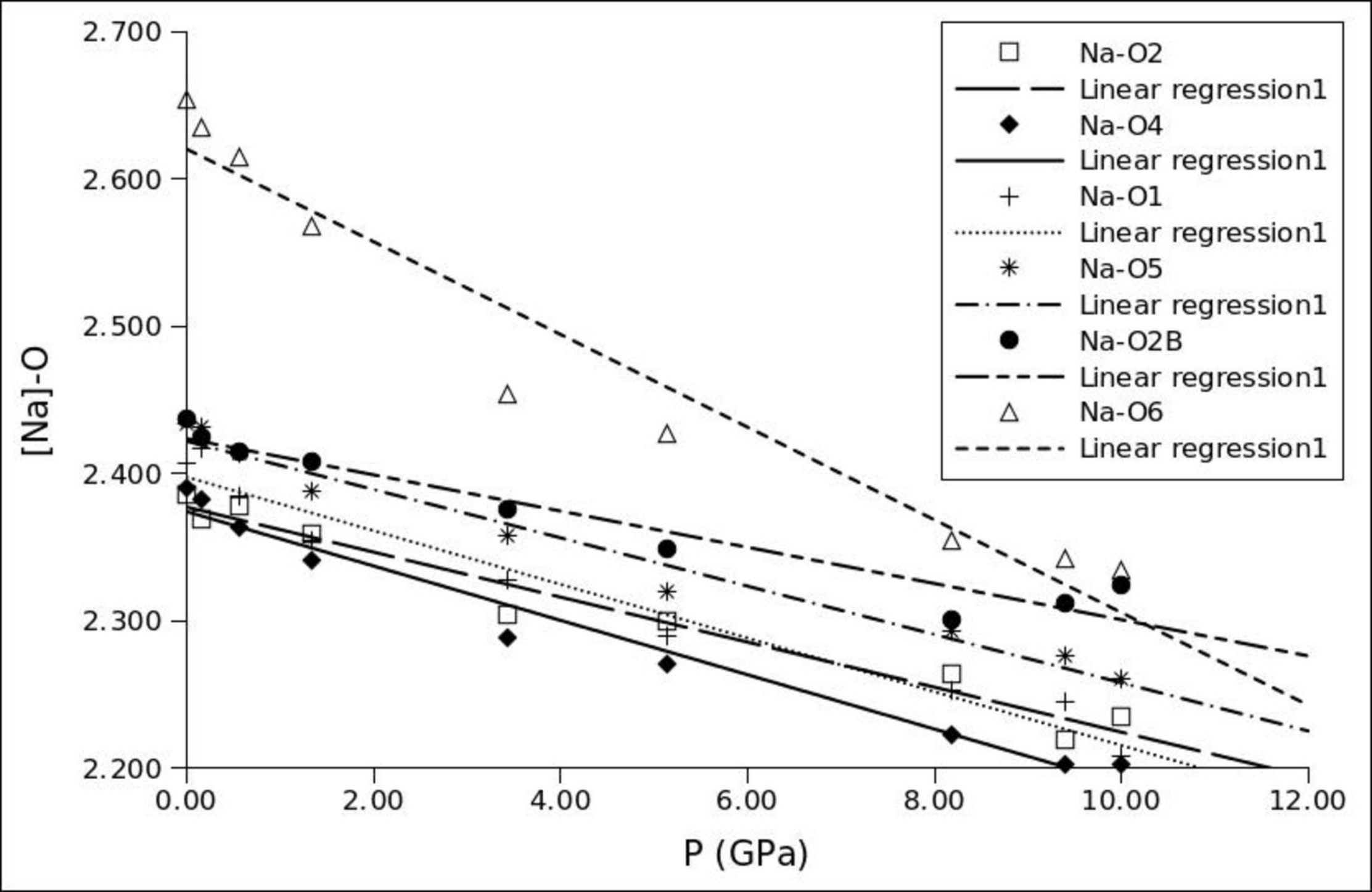
2.700
2.600
2.500
2.400
2.300
2.200
[Na]-O
0.00
2.00
4.00
6.00
8.00
10.00
12.00
P (GPa)
Na-O2
Linear regression1
Na-O4
Linear regression1
Na-O1
Linear regression1
Na-O5
Linear regression1
Na-O2B
Linear regression1
Na-O6
Linear regression1

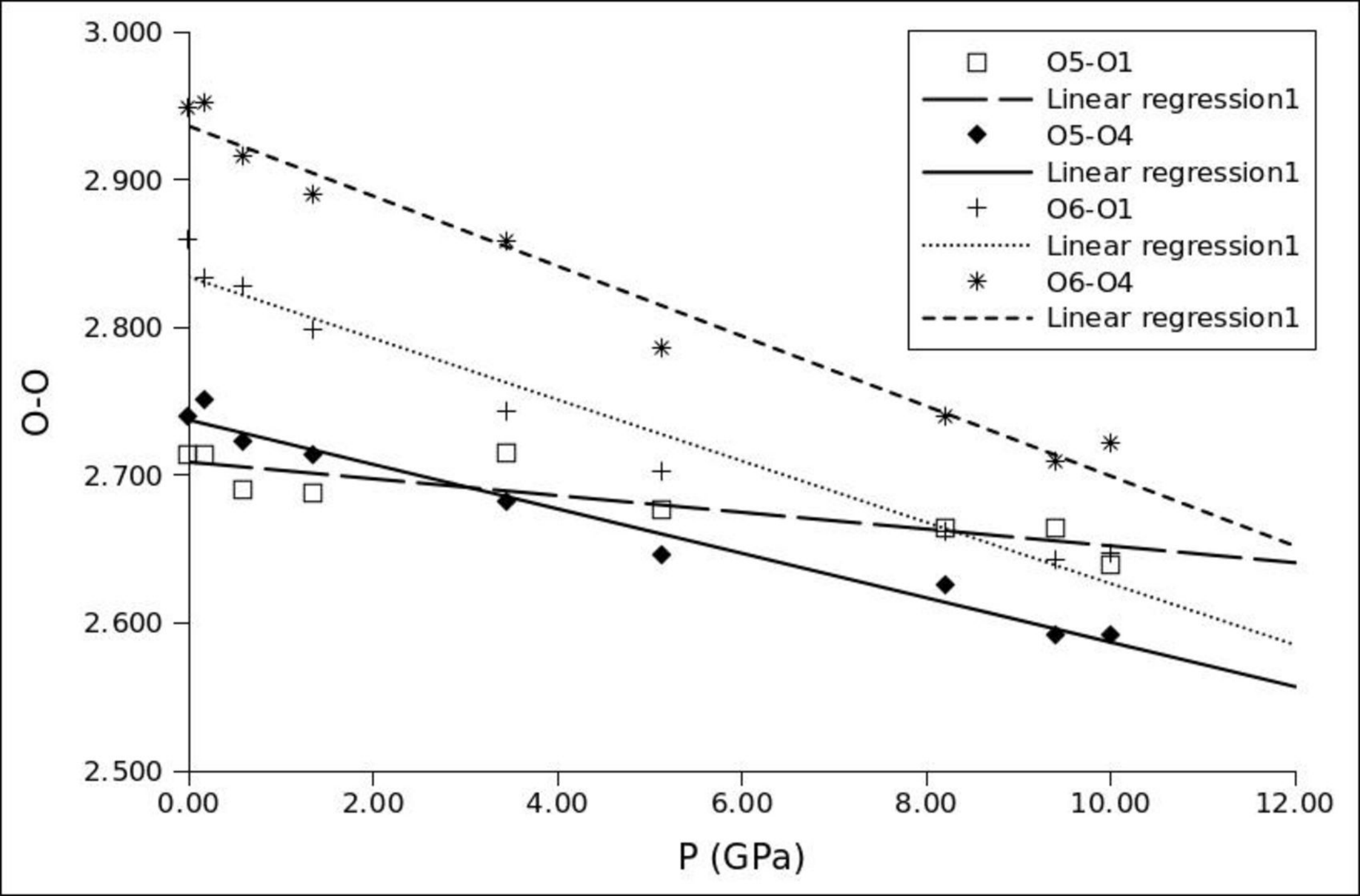
3.000
2.900
2.800
2.700
2.600
2.500
O-O
0.00
2.00
4.00
6.00
8.00
10.00
12.00
P (GPa)
O5-O1
Linear regression1
O5-O4
Linear regression1
O6-O1
Linear regression1
O6-O4
Linear regression1

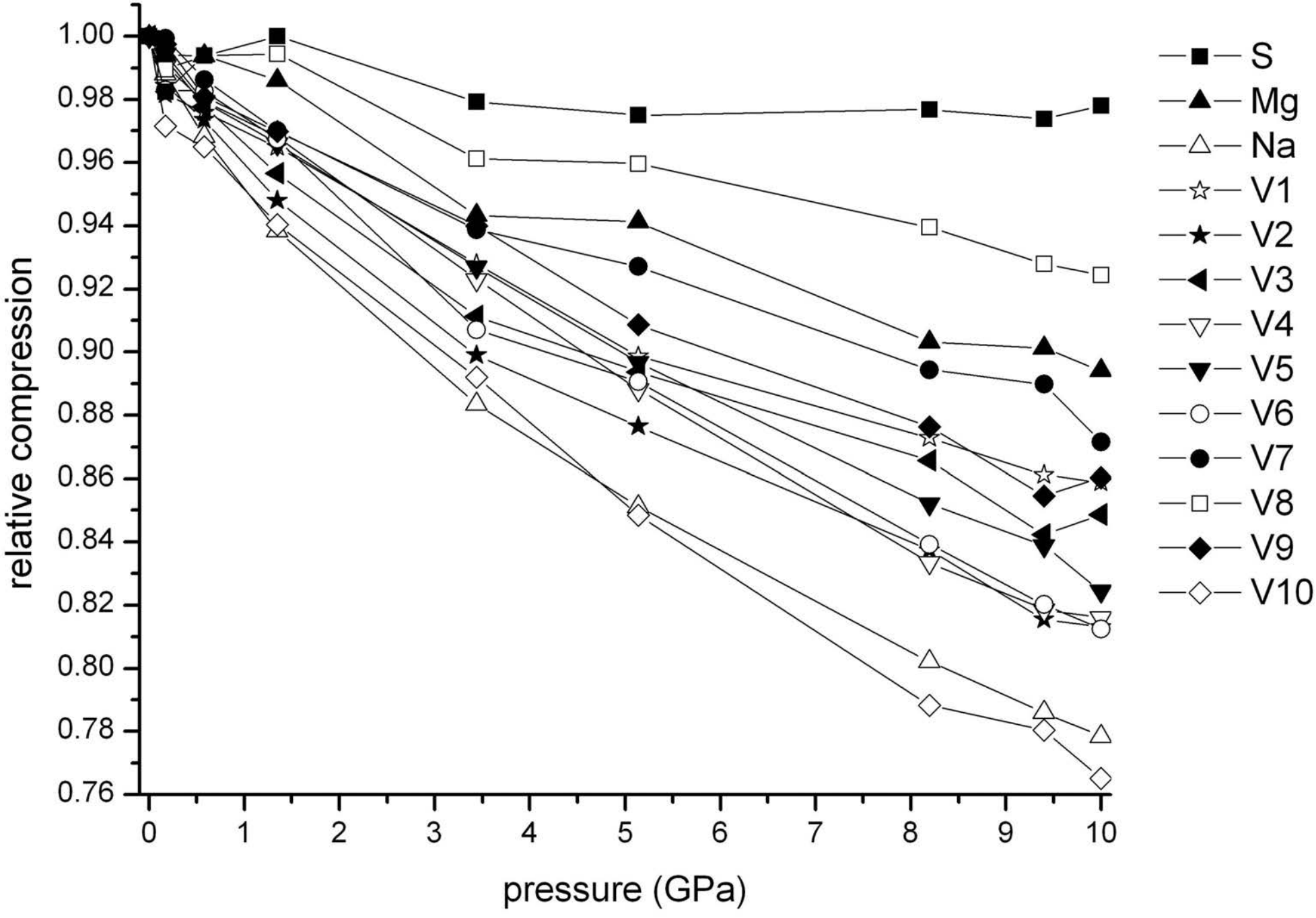
relative compression
1.00
0.98
0.96
0.94
0.92
0.90
0.88
0.86
0.84
0.82
0.80
0.78
0.76
0
1
2
3
4
5
6
7
8
9
10
pressure (GPa)
S
Mg
Na
V1
V2
V3
V4
V5
V6
V7
V8
V9
V10

Table 1.

Pressure (GPa)	0.001	0.17	0.58	1.35	2.07	3.44	5.14	5.95	8.2	9.4	10	11.2
Data collection												
2θmax (°)	59.97	37.33	38.19	37.48	37.93	36.24	37.76	38.16	36.82	37.00	38.08	38.13
No. Measured reflections	3073	732	948	800	914	688	650	853	614	616	838	793
No. Unique reflections	1266	465	544	471	506	427	422	474	400	385	452	434
No. Obs. reflections [Fo>4σ(Fo)]	1029	319	330	341	315	202	229	189	211	185	152	136
R_{int}	0.0136	0.0433	0.0687	0.0570	0.0936	0.1275	0.0457	0.1366	0.0487	0.0869	0.1321	0.1579
R_{σ}	0.0200	0.0399	0.0550	0.0474	0.0691	0.1111	0.0617	0.1161	0.0706	0.1006	0.1389	0.1522
Range *h,k,l*	-15 ≤ h ≤ 14	-14 ≤ h ≤ 12	-13 ≤ h ≤ 15	-14 ≤ h ≤ 13	-14 ≤ h ≤ 14	-14 ≤ h ≤ 12	-14 ≤ h ≤ 12	-14 ≤ h ≤ 14	-14 ≤ h ≤ 12	-14 ≤ h ≤ 12	-14 ≤ h ≤ 14	-14 ≤ h ≤ 13
	-11 ≤ k ≤ 10	-9 ≤ k ≤ 11	-10 ≤ k ≤ 11	-10 ≤ k ≤ 11	-10 ≤ k ≤ 10	-9 ≤ k ≤ 10	-9 ≤ k ≤ 10	-9 ≤ k ≤ 10	-9 ≤ k ≤ 10	-9 ≤ k ≤ 10	-9 ≤ k ≤ 10	-9 ≤ k ≤ 10
	-7 ≤ l ≤ 6	-5 ≤ l ≤ 6	-6 ≤ l ≤ 6	-5 ≤ l ≤ 6	-5 ≤ l ≤ 6	-5 ≤ l ≤ 5	-5 ≤ l ≤ 5	-5 ≤ l ≤ 6	-4 ≤ l ≤ 5	-4 ≤ l ≤ 5	-5 ≤ l ≤ 6	-4 ≤ l ≤ 6
Structure Refinement												
No. Parameters	97	36	36	36		36	36		36	36	36	
R_1 (F > 4σ)	0.0214	0.0621	0.0492	0.065		0.0681	0.0513		0.0411	0.0514	0.0485	
wR_2	0.0644	0.1968	0.3094	0.2021		0.2436	0.179		0.127	0.1611	0.4576	
GooF	1.077	1.115	1.854	1.105		1.166	1.068		0.962	0.955	1.754	
Highest peak	0.32	0.49	0.83	0.54		0.87	0.4		0.37	0.44	1.79	
Deepest hole	−0.34	−0.56	−0.58	−0.51		−0.85	−0.44		−0.26	−0.44	−0.89	

Table 3

P (GPa)	0.00	0.17	0.58	1.35	2.07	3.44	5.14	5.95	8.20	9.40	10.0	11.2
***a*(Å)**	11.115(9)	11.091(2)	11.056(2)	11.003(2)	10.948(2)	10.860(2)	10.770(3)	10.739(3)	10.649(8)	10.621(3)	10.613(3)	10.576(3)
***b* (Å)**	8.242(2)	8.216(1)	8.178(1)	8.124(1)	8.075(1)	7.985(1)	7.910(2)	7.876(2)	7.810(5)	7.783(1)	7.772(2)	7.754(2)
***c* (Å)**	5.538(1)	5.518(1)	5.500(1)	5.465(1)	5.432(1)	5.376(2)	5.316(2)	5.268(2)	5.209(4)	5.158(2)	5.137(2)	5.079(2)
***β* (°)**	100.82(4)	100.71(2)	100.73(2)	100.64(2)	100.55(2)	100.55(2)	100.40(2)	100.45(3)	100.43(7)	100.49(2)	100.57(3)	100.64(3)
***V* (Å^3)**	498.4(7)	494.1(2)	488.7(1)	480.2(2)	472.1(1)	458.3(2)	445.5(2)	439.8(2)	426.0(6)	419.3(2)	416.5(2)	409.3(2)
***ρ* (g/cm^3)**	1.196	1.206	1.219	1.241	1.262	1.300	1.338	1.360	1.398	1.421	1.430	1.455
***μ* (mm^{-1})**	0.41	0.21	0.21	0.22	0.22	0.23	0.23	0.24	0.25	0.25	0.25	0.26

Table 4

	x	*y*	*z*	U11	U22	U33	U23	U13	U12	Ueq/iso
Na	0.36164(6)	0.07028(8)	0.1307(1)	0.0181(4)	0.0206(4)	0.0237(4)	-0.0014(2)	0.0023(3)	0.0013(2)	0.0210(3)
Mg	0.0	0.0	0.0	0.0115(3)	0.0123(3)	0.0135(4)	-0.0003(2)	0.0023(2)	-0.0009(2)	0.0124(2)
S	0.13640(3)	0.29068(4)	0.36948(6)	0.0120(2)	0.0126(2)	0.0117(2)	0.0003(1)	0.0015(1)	-0.0010(1)	0.0122(1)
O1	0.2662(1)	0.2714(1)	0.3473(2)	0.0132(5)	0.0218(5)	0.0286(7)	0.0017(4)	0.0057(4)	0.0019(4)	0.0210(3)
O2	0.0801(1)	0.4210(1)	0.2094(2)	0.0168(6)	0.0249(6)	0.0249(6)	0.0108(5)	0.0027(5)	0.0036(4)	0.0223(3)
O3	0.0706(1)	0.1372(1)	0.3057(2)	0.0248(6)	0.0194(5)	0.0179(6)	-0.0039(4)	0.0033(4)	-0.0101(4)	0.0208(3)
O4	0.1322(1)	0.3284(1)	0.6291(2)	0.0334(7)	0.0194(5)	0.0139(6)	-0.0040(4)	0.0063(4)	-0.0031(5)	0.0220(3)
O5	0.1601(1)	0.0379(2)	0.8733(2)	0.0178(6)	0.0168(5)	0.0176(6)	0.0003(5)	0.0069(4)	0.0004(4)	0.0169(2)
O6	0.0810(1)	0.7913(1)	0.1771(2)	0.0178(6)	0.0172(5)	0.0195(6)	0.0023(4)	-0.0022(5)	-0.0019(4)	0.0189(3)
H5A	0.155(2)	0.115(3)	0.792(5)							0.035(6)
H5B	-0.173(3)	0.023(4)	0.203(6)							0.042(8)
H6A	0.452(3)	0.231(4)	0.797(6)							0.05(1)
H6B	-0.133(2)	0.200(3)	-0.298(6)							0.032(6)

Table 5

Pressure (GPa)		0.17	0.58	1.35	3.44	5.14	8.2	9.4	10
Atomic positions									
Na	*x*	0.3623(4)	0.3615(3)	0.3613(3)	0.3635(7)	0.3636(5)	0.3661(4)	0.3674(5)	0.3672(6)
	y	0.0710(4)	0.0723(4)	0.0748(4)	0.0797(8)	0.0829(5)	0.0878(4)	0.0890(6)	0.0889(7)
	z	0.1302(8)	0.1300(8)	0.1298(8)	0.127(2)	0.126(1)	0.1240(9)	0.123(1)	0.126(1)
Mg	*x*	0	0	0	0	0	0	0	0
	y	0	0	0	0	0	0	0	0
	z	0	0	0	0	0	0	0	0
S	*x*	0.1364(2)	0.1365(2)	0.1367(2)	0.1364(3)	0.1366(3)	0.1368(3)	0.1373(3)	0.1372(4)
	y	0.2914(2)	0.2916(2)	0.2921(2)	0.2924(4)	0.2945(3)	0.2953(3)	0.2958(4)	0.2968(4)
	z	0.3709(4)	0.3726(4)	0.3747(5)	0.3803(7)	0.3842(6)	0.3913(6)	0.3939(7)	0.3971(9)
O1	*x*	0.2656(6)	0.2670(6)	0.26783(7)	0.269(1)	0.2688(9)	0.2691(7)	0.2686(9)	0.270(1)
	y	0.2726(7)	0.2721(7)	0.2719(7)	0.271(1)	0.2695(9)	0.2691(8)	0.268(1)	0.268(1)
	z	0.349(1)	0.350(1)	0.352(1)	0.359(3)	0.361(2)	0.362(1)	0.363(2)	0.359(2)
O2	*x*	0.0796(7)	0.0804(6)	0.0795(6)	0.079(1)	0.0805(9)	0.0815(8)	0.079(1)	0.080(1)
	y	0.4227(7)	0.4230(7)	0.4246(7)	0.427(1)	0.4284(9)	0.4339(8)	0.436(1)	0.436(1)
	z	0.210(2)	0.209(1)	0.209(2)	0.214(3)	0.213(2)	0.218(2)	0.225(2)	0.227(3)
O3	*x*	0.0704(6)	0.0707(6)	0.0696(6)	0.068(1)	0.0674(8)	0.0637(7)	0.0637(9)	0.062(1)
	y	0.1373(7)	0.1371(7)	0.1376(7)	0.138(1)	0.1364(9)	0.1376(8)	0.1392(9)	0.138(1)
	z	0.307(1)	0.309(1)	0.312(1)	0.320(2)	0.324(2)	0.333(2)	0.337(2)	0.337(2)
O4	*x*	0.1339(7)	0.1325(6)	0.1316(7)	0.133(1)	0.1344(8)	0.1383(7)	0.1400(8)	0.142(1)
	y	0.3301(7)	0.3306(7)	0.3325(7)	0.337(1)	0.3371(8)	0.3408(8)	0.3409(9)	0.339(1)
	z	0.628(2)	0.632(1)	0.636(1)	0.646(2)	0.652(2)	0.666(2)	0.675(2)	0.675(3)
O5	*x*	0.1599(6)	0.1609(6)	0.1617(6)	0.161(1)	0.1642(8)	0.1645(7)	0.1661(9)	0.167(1)
	y	0.0380(7)	0.0384(6)	0.0392(6)	0.041(1)	0.0403(8)	0.0400(7)	0.0406(9)	0.039(1)
	z	0.876(1)	0.873(1)	0.877(1)	0.886(3)	0.885(2)	0.894(2)	0.895(2)	0.899(2)
O6	*x*	0.0810(6)	0.0804(6)	0.0810(6)	0.081(1)	0.0785(7)	0.0758(7)	0.0741(8)	0.0744(9)
	y	0.7897(6)	0.7891(6)	0.7878(6)	0.786(1)	0.7845(9)	0.7846(8)	0.7854(9)	0.784(1)
	z	0.180(1)	0.178(1)	0.177(1)	0.172(2)	0.176(2)	0.176(2)	0.178(2)	0.176(2)
Atomic displacement factors (Uiso) (Å^2)									
Na		0.022(2)	0.017(1)	0.015(1)	0.013(2)	0.017(2)	0.014(1)	0.015(2)	0.018(2)
Mg		0.014(1)	0.0121(9)	0.0115(9)	0.011(2)	0.013(1)	0.012(1)	0.011(1)	0.013(2)
S		0.0149(7)	0.0128(6)	0.0130(7)	0.010(1)	0.013(1)	0.0115(7)	0.0114(9)	0.011(1)
O1		0.022(1)	0.020(1)	0.020(1)	0.015(3)	0.017(2)	0.016(1)	0.015(2)	0.014(2)
O2		0.025(2)	0.020(1)	0.020(1)	0.019(3)	0.021(2)	0.018(2)	0.020(2)	0.020(3)
O3		0.022(2)	0.020(1)	0.022(2)	0.015(3)	0.019(2)	0.017(2)	0.015(2)	0.017(3)
O4		0.027(2)	0.021(1)	0.022(1)	0.018(3)	0.018(2)	0.017(2)	0.018(2)	0.018(2)
O5		0.021(1)	0.021(1)	0.017(1)	0.015(3)	0.017(2)	0.016(2)	0.012(2)	0.010(2)
O6		0.020(1)	0.017(1)	0.018(1)	0.014(2)	0.015(2)	0.014(1)	0.011(2)	0.011(2)

Table 6

Pressure (GPa)	0.00	0.17	0.58	1.35	3.44	5.14	8.2	9.4	10
O5-O1	2.71(1)	2.71(1)	2.69(1)	2.69(1)	2.72(1)	2.68(1)	2.66(1)	2.66(1)	2.64(1)
O5-O4	2.74(1)	2.75(1)	2.72(1)	2.71(1)	2.68(1)	2.65(1)	2.63(1)	2.59(1)	2.59(1)
O6-O1	2.86(1)	2.83(1)	2.83(1)	2.80(1)	2.74(1)	2.70(1)	2.66(1)	2.64(1)	2.65(1)
O6-O4	2.95(1)	2.95(1)	2.92(1)	2.89(1)	2.86(1)	2.79(1)	2.74(1)	2.71(1)	2.72(1)
Na-O2A	2.386(2)	2.368(8)	2.378(7)	2.359(7)	2.30(2)	2.30(1)	2.26(1)	2.22(1)	2.23(2)
Na-O4	2.391(1)	2.382(8)	2.363(7)	2.341(8)	2.29(1)	2.270(9)	2.222(8)	2.20(1)	2.20(1)
Na-O1	2.407(2)	2.42(1)	2.384(9)	2.35(1)	2.33(2)	2.29(1)	2.25(1)	2.24(1)	2.21(2)
Na-O5	2.433(2)	2.432(6)	2.413(6)	2.388(6)	2.36(1)	2.320(8)	2.292(7)	2.276(8)	2.261(9)
Na-O2B	2.437(1)	2.42(1)	2.415(9)	2.41(1)	2.38(2)	2.35(1)	2.30(1)	2.31(1)	2.32(2)
Na-O6	2.653(2)	2.635(9)	2.614(8)	2.568(9)	2.45(2)	2.43(1)	2.35(1)	2.34(1)	2.33(2)
<Na-O>	2.45(1)	2.44(1)	2.43(9)	2.40(8)	2.35(6)	2.33(6)	2.28(5)	2.27(5)	2.26(6)
V_{Na}	18.42(3)	18.2(1)	17.8(1)	17.3(1)	16.3(1)	15.7(1)	14.8(3)	14.5(1)	14.3(2)
asp (vol)	7.7%	7.5%	6.7%	5.7%	2.8%	2.7%	1.0%	1.8%	1.5%
vd	5.4%	5.4%	5.5%	5.4%	5.3%	5.7%	6.0%	6.0%	5.8%
ecc (vol)	15.2%	14.7%	14.6%	13.7%	11.1%	10.0%	9.3%	11.0%	11.3%
Mg-O5 x 2	2.056(2)	2.040(9)	2.052(8)	2.040(9)	1.98(2)	2.00(1)	1.95(1)	1.96(1)	1.96(1)
Mg-O3 x 2	2.064(1)	2.066(6)	2.062(6)	2.063(6)	2.06(1)	2.049(8)	2.049(7)	2.055(9)	2.04(1)
Mg-O6 x 2	2.097(1)	2.108(5)	2.097(5)	2.093(5)	2.063(9)	2.053(7)	2.015(6)	1.997(7)	2.000(8)
<Mg-O>	2.07(2)	2.07(2)	2.07(2)	2.07(3)	2.04(4)	2.03(3)	2.01(5)	2.00(5)	2.00(4)
V_{Mg}	11.856(2)	11.87(2)	11.82(2)	11.73(2)	11.22(2)	11.20(7)	10.76(6)	10.72(7)	10.68(6)
asp (vol)	2.7%	4.5%	3.1%	3.5%	5.9%	4.0%	6.4%	6.3%	5.4%
vd	0.1%	0.1%	0.1%	0.1%	0.2%	0.1%	0.2%	0.2%	0.2%
S-O2	1.457(1)	1.463(7)	1.462(6)	1.470(6)	1.46(1)	1.454(9)	1.463(7)	1.461(9)	1.45(1)
S-O3	1.471(1)	1.472(6)	1.468(6)	1.464(6)	1.45(1)	1.462(8)	1.459(7)	1.449(8)	1.467(9)
S-O1	1.479(2)	1.468(9)	1.481(8)	1.486(9)	1.47(2)	1.46(1)	1.46(1)	1.45(1)	1.48(1)
S-O4	1.480(1)	1.46(1)	1.473(8)	1.477(9)	1.47(1)	1.47(1)	1.47(1)	1.49(1)	1.46(1)
<S-O>	1.47(1)	1.466(5)	1.471(8)	1.474(9)	1.46(1)	1.462(6)	1.463(6)	1.46(2)	1.46(1)
V_S	1.636(6)	1.626(8)	1.630(8)	1.641(9)	1.61(2)	1.60(2)	1.61(3)	1.60(3)	1.61(4)
vd	0.02%	0.07%	0.02%	0.04%	0.03%	0.05%	0.07%	0.05%	0.05%
ecc (vol)	3.5%	1.8%	2.4%	2.8%	3.3%	1.6%	2.0%	5.6%	3.5%